Acta Scientiarum
http://periodicos.uem.br/ojs/acta
ISSN on-line: 1807-8664
Doi: 10.4025/actascitechnol.v41i1.41103

The influence of glycerol as an additive in Zinc-Manganese alloy coatings formed by electrodeposition

Eliene Leandro de Araújo[1,2], Alisson Mendes Rodrigues[3], Anderson Bezerra Viana[4] and Rommel Bezerra Viana[2,5*]

[1]Departamento de Química, Universidade Federal de São Carlos, São Carlos, São Paulo, Brazil. [2]Instituto de Química de São Carlos, Universidade de São Paulo, São Carlos, São Paulo, Brazil. [3]Departamento de Engenharia de Materiais, Universidade Federal de São Carlos, São Carlos, São Paulo, Brazil. [4]Departamento de Engenharia Oceânica, Centro de Tecnologia, Instituto Alberto Luiz Coimbra de Pós-Graduação e Pesquisa de Engenharia, Universidade Federal do Rio de Janeiro, Rio de Janeiro, Rio de Janeiro, Brazil. [5]Instituto de Química. Universidade Federal de Alfenas, Alfenas, Minas Gerais, Brazil. *Author for correspondence. E-mails: rommelbv@yahoo.com.br

ABSTRACT. The aim of this investigation is to evaluate the influence of glycerol (a nontoxic additive) on Zn-Mn coatings formed by electrochemical deposition. The influence of glycerol (GLY) on the electrodeposition of Zn-Mn alloys on Pt from acid baths was studied by cyclic voltammetry. The coatings were analyzed by scanning electron microscopy (SEM) and X-ray diffraction (XRD). The Zn-Mn alloys prepared in the absence or presence of this additive showed similar voltammograms except when using GLY and boric acid (BA) concentrations at 0.63 and 0.24 M, respectively. The current efficiency of the Zn-Mn electrodeposition process ranged from 5 to 41%, due to the lowest and highest concentrations of GLY and BA, respectively. SEM images of deposits obtained at -1.53 V from baths containing 0.08-0.48 M GLY were dendritic, while those formed in the presence of 0.63 M GLY showed that GLY acted as a brightener at this concentration. The XRD analysis showed that the electrodeposits contained Zn, Mn, oxides as well as alloys of various compositions. GLY acted as a grain refiner and inhibited the codeposition of Zn with Mn and the formation of oxides.

Keywords: electrodeposition; Zn-Mn alloy; polyalcohol; cyclic voltammetry.

Received on December 27, 2017.
Accepted on April 13, 2018

Introduction

Electrodeposited alloys of Zn–Mn are thermodynamically nobler and more durable than pure Zn coatings (Díaz-Arista et al., 2009; Touazi et al., 2016). These Zn-Mn alloys have been extensively studied (Bozzini et al., 2011; Bucko, Mišković-Stanković, Rogan, & Bajat, 2015; Bucko, Rogan, Stevanovic, Stankovic, & Bajat, 2013a; Close et al., 2016; Ganesan, Prabhu, & Popov, 2014; Griskonis, Fanigliulo, & Sulcius, 2002; Fashu et al., 2015; Marin-Sanchez, Ocon, Conde, & Garcia, 2014; Wykpis, Bierska-Piech, & Kubisztal, 2014) because they offer good corrosion resistance (Bozzini et al. 1999; Claudel et al., 2019; Ganesan et al., 2014; Louki & Feki, 2017a, 2017b), weldability, paintability (Fashu et al., 2015), appearance (Silva, Schmitz, Spinelli, & Garcia, 2012), mechanical properties, particularly plasticity (Bozzini et al., 1999) as well as hardness, tensile and compressive strength and improved passivation behavior in chloride medium (Bozzini et al., 1999; Díaz-Arista et al., 2009; Bucko, Lacnjevac, & Bajat, 2013b). Furthermore, there is a particular interest in these Zn-Mn alloys in the automotive industry (Ananth & Parthasaradhy, 1996; Muller, Sarret, & Andreu, 2003a; 2003b; Silva et al., 2012) and for steel cable and plate coatings because they offer better adhesion between steel and polymer blends and easy adhesion of paint-even when the Mn content is low (Bozzini et al., 1999).

It is interesting to note that there are some fundamental difficulties in electrodeposition of Zn-Mn alloys that is related to the very negative reduction potential of manganese in aqueous solutions [-1.18 V (vs. NHE)]. This is considerably more negative than that of zinc, -0.76 V (vs. NHE) (Brenner, 1963). This higher electronegativity of Mn confers two types of protection on the steel: it dissolves prior to Zn (Boshkov, Petrov, & Vitkova, 2002; Boshkov, Petrov, Vitkova, & Raichevsky, 2005; Díaz-Arista et al., 2009; Chen & Hussey, 2007) and it also ensures better protective ability with low solubility products (Wykpis et al., 2014). Moreover, this Mn electronegativity leads to significant but low efficiency hydrogen evolution reaction (HER) (Bozzini et al., 1999; Díaz-Arista et al., 2009). According to Ananth and Parthasaradhy (1996), the Zn-Mn system is so complex that the Mn content in the alloy can range from 0 to 100%.

Additives such as thiourea (Sulcius, Griskonis, & Diaz-Arista, 2009), selenous acid and ammonium selenate (Griskonis & Sulcius, 2005), sulphate, sulphate-citrate (Wilcox & Gabe, 1993; Bozzini et al., 2002), thiocarbamide (Bozzini et al., 2002), EDTA-citrate (Muller et al., 2003a; 2003b), polyethylene glycol (Ortiz, Diaz-Arista, Meas, Ortega-Borges, & Trejo, 2009), cyanide, ammonium thiocyanate (Díaz-Arista et al., 2009; Ortiz et al., 2009; Close et al., 2016), fluoroborate (Bucko et al., 2011), chloride (Claudel et al. 2019; Ganesan et al., 2014; Louki & Feki, 2017a, 2017b; Marin-Sanchez et al., 2014; Sylla et al., 2005) and different solvents (Bucko et al, 2017,2018; Chung et al., 2008) have been shown to affect the manganese content in the electrodeposit (Wilcox & Gabe, 1993; Bucko et al., 2013a). Nevertheless, these electrolytes have limitations including instability (Brenner, 1963), toxicity (Wilcox & Gabe, 1993), corrosiveness and precipitation of the Mn (Bozzini et al., 1999; Bucko et al., 2015; Silva et al., 2012). The influence of boric-sorbitol complex (BSC) (Rubin, Oliveira, & Carlos, 2012) on the composition of the Zn-Mn alloy was studied, and this additive inhibited the deposition of manganese.

The aim of this investigation is to describe the development and stable deposition bath based on boric acid (BA) and glycerol (GLY). Because GLY possesses fewer hydroxyls than sorbitol, it is expected that this bath will act differently than the BSC bath. On the other hand, baths containing GLY are less harmful to the environment than those containing the toxic additives mentioned above; their residues are more easily treated. To achieve a fundamental understanding of the electrodeposition process of Zn-Mn alloys on Pt substrate, potentiodynamic curves were recorded and the deposits were subjected to morphological, chemistry and structural analysis by scanning electron microscopy (SEM) and X-ray diffraction (XRD).

Material and methods

All experiments were carried out at room temperature (~25ºC) in a 50 mL glass single-compartment cell. All chemicals were of analytical grade and deionized water was used. A Pt disk (0.196 cm^2), Pt plate and a calomel electrode (Hg/Hg_2Cl_2, KCl 1.0 M) were employed as the working, auxiliary and reference electrodes, respectively.

Immediately prior to the electrochemical measurements, the working electrode was polished with 0.3 μm alumina powder to a mirror finish dipped in a mixture of concentrated sulfuric and nitric acids and then rinsed with distilled water. The deposition baths were composed of BA, zinc and manganese sulfates in the presence of the GLY additive whose concentrations are described in Table 1. GLY was added to A-F baths at proportions of 1:1, 1:2, 1:3, 1:4, 1:6 and ~1:8, with respect to BA. This was done to facilitate comparisons with studies previously carried out with sorbitol at these concentrations [0.16 M and 0.48 M]. In baths G and H, the concentration of boric acid (BA) was three times that of A-F. In F and H (with the highest concentration of GLY), the proportion of this additive was not exact because the solution of GLY was saturated.

To allow better comparison between the voltammograms, the bath pH was adjusted to ~3.20 with sulfuric acid. At this pH, no mold developed, and the bath remained stable and clean. Additive-free solutions without GLY but with all other reagents were also prepared. Potentiodynamic curves were recorded with a GAMRY PCI-4750 mA potentiostat/galvanostat, which was evaluated by a triplicate analysis. In the potentiostatic tests, the Zn-Mn alloys were deposited at -1.53 V with a deposition charge densities of 10.20 C cm^{-2}. These deposits were stripped in a solution of 0.030 M HNO_3 at a sweep rate of 10 mV s^{-1}, and the current efficiency (CE) was calculated from the stripping/deposition charge ratio. SEM photographs were taken with a Phillips (model XL 30FEG) electron microscope. The EDS measurements were made with an Oxford Instruments LINK ISIS microscope. XRD patterns were collected with a Rigaku diffractometer with Rotaflex RU200B X-ray goniometer operating with Cu Kα radiation (λ = 1.5406 Å) in a range of 2θ from 30 to 90° with scan rate of 2º $min.^{-1}$.

Table 1. Concentration (in M) of the components in the deposition baths.

Baths	$ZnSO_4$	$MnSO_4$	BA	GLY
(A)	0.10	0.14	0.08	0.08
(B)	0.10	0.14	0.08	0.16
(C)	0.10	0.14	0.08	0.24
(D)	0.10	0.14	0.08	0.32
(E)	0.10	0.14	0.08	0.48
(F)	0.10	0.14	0.08	0.63
(G)	0.10	0.14	0.24	0.48
(H)	0.10	0.14	0.24	0.63

Results and discussion

Potentiodynamic studies of Zn-Mn electrodeposits

To investigate the process of electroplating, the Zn-Mn voltammograms were recorded on a Pt substrate in deposition baths containing salts of Mn and Zn with boric acid (BA) and glycerol (GLY) at various concentrations. Figure 1 shows cyclic voltammetric curves for Pt in electrolytic solutions with six different concentrations of GLY (baths A-F, see Table 1). There are two cathodic peaks in the negative sweep (Figure 1a, inset) named c_1 and c_2. In the positive sweep, an anodic peak a_1 (E_{pa1}~-0.70 V) and an anodic region a_2 (between +0.41 and +1.32 V) can be seen. Thus, peaks a_1 and a_2 refer to the dissolution and passivation of the deposit and the formation of manganese oxide, respectively. We visually observed a light gray film on the electrode at the end of the anodic peak a_1. A reddish-brown coloration was seen in the film while at the end of region a_2, which may be due to manganese oxide (MnO_2) (Pourbaix, 1966). It is interesting to note that this a different picture from what was observed in initial tests without the addition of Mn. In this case, no significant changes took place in the voltammetric profile among different concentrations of GLY (see Table 1), while the reduction process was depolarized by the increase of BA.

The c_1 peak has a potential (E_{cp1}) that remains practically constant (~-1.32 V) up to 0.32 M GLY (bath D) (see Figure 1, inset). Nevertheless, a shift to more negative values was observed at higher concentrations of GLY ($\geqslant$ 0.48 M). There were shifts of ~40 and ~20 mV in the negative direction when the GLY concentration was increased from bath A to F. The current density of peak c_1 decreased from 11.68 (bath A) to 10.14 mA cm^{-2} (bath F).

The potential of peak c_2 (E_{cp2}) shifted ~20 mV in the negative direction when the GLY concentration increased from 0.08 to 0.48 M and ~40 mV to 0.63 M. However, the increase in current density of this peak (j_{cp2}) was more significant at GLY concentrations exceeding 0.32 M. The significant increase in j_{cp2} with rising GLY content is due to the intense HER ($2H_3O^+_{(aq)}+2e^-\rightarrow H_{2(g)}+2H_2O_{(aq)}$) that occurred in parallel with the reduction of Zn and Mn in the region of peak c_2. These results imply that the adsorption of the additives BA and GLY on the electrodeposits lead to a decrease in j_{cp1} and a shift in E_{cp2} to more negative values with increasing of GLY.

GLY hindered the Zn-Mn dissolution process. This was probably by adsorption on the electrodeposits because j_{ap1} decreased (~20.0 to 7.53 mA cm^{-2}) as the GLY concentration bath increased (0.0 to 0.63 M). Also, the formation of oxides (in region a_2) was strongly inhibited by GLY as shown in the decreasing of j_{ap2}. However, the passive region between peaks a_1 and a_2 was not affected by the GLY concentration.

At higher concentrations of additives (baths G and H, see Figure 1), the peak c_2 was observed for bath G but not for bath H. This is probably because peak c_2 was shifted to a region of potential with high HER, ~-1.80 V. There were generally no significant differences between baths G and H in the cathodic peak potential (E_{cp1}) or anodic peak potential (E_{ap1}). However, the current density (j_{ap1}) increased from 11.28 (bath G) to 12.10 mA cm^{-2} (bath H). The dissolution of the deposit and deposition of Zn with Mn were hindered by raising the GLY concentration. The resulting deposits were adherent and dark gray at the end of the voltammetric sweep.

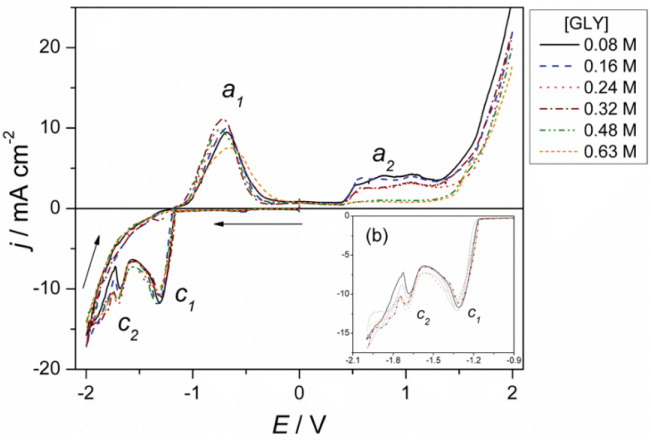

Figure 1. Voltammetric curves (v = 10 mV s^{-1}) for Pt in $ZnSO_4$ (0.10 M) + $MnSO_4$ (0.14 M) + BA (0.08 M) at various concentrations of glycerol (inset: Expanded negative sweep).

Deposition voltammograms were generated by changing the concentration of BA from 0.08 M to 0.24 M for the same GLY concentration (0.48 M, see Figure 2) to observe the individual effects of the BA content. The cathodic peak potential (E_{cp1}) shifted from -1.35 V (0.08 M BA) to -1.31 V (0.24 M BA), while the current density for this peak decreased from 11.44 to 10.33 mA cm^{-2}. The E_{cp2} peak shifted 80 mV to more negative values, and the current density (j_{cp2}) increased significantly from 11.20 to 15.77 mA cm^{-2}. E_{ap1} did not change significantly, but the anodic current density increased from 9.93 to 11.28 mA cm^{-2}. This confirms the fact that the glycerol hindered the dissolution of Zn-Mn deposit.

It can be noted that the same BA content increase was maintained as in previous baths (from 0.08 to 0.24 M), however the GLY concentration was increased to 0.63 M (baths F and H, see Figure 3). No obvious modification was observed in the voltammetric profile except that peak c_2 was not observed. At 0.08 M BA, this peak occurred at -1.72 V (j_{pc2} = 11.22 mA cm^{-2}). At 0.24 M BA, the same peak was shifted to the HER region. At 0.08 M BA with 0.48 to 0.63 M GLY, the j_{a2} decreased more significantly than in the corresponding baths containing 0.24 M BA. At the start of the potential, this region shifted to more positive values confirming that the GLY inhibited the formation of Mn oxides. Nevertheless, j_{a2} remained contstant when BA was 0.24 M and the GLY concentration was raised from 0.48 to 0.63 M in the bath. Therefore, at these concentrations, GLY significantly inhibited manganese oxide formation (region a_2) when the BA concentration was 0.08 M.

The deposition of Zn-Mn in the absence and presence of various concentrations of GLY show similar voltammetric curves. Here, E_{cp2} shifted to more negative values as the GLY concentration increased. Glycerol inhibited the reduction of Zn and Mn, and this inhibition was more significant at concentrations > 0.32 M. Moreover, the j_{cp1} decreased while j_{cp2} increased in the presence of the glycerol additive. The dissolution process was not affected (E_{ap1}) except in bath H, where j_{a1} increased from 8.19 (without GLY) to 12.10 mA cm^{-2} (with GLY).

The deposition process from baths containing GLY was further investigated by the reversed sweep technique (see Figure 2). When the range of potential went more negative than -1.18 V (region c_o), an anodic peak (a') of the oxidation of the molecular hydrogen (H_2) was retained on the Pt electrode. The peak disappeared when the voltammogram was recorded in a stirred electrolyte (Figure 2, inset). In addition, two crossovers could be seen in the reversed sweep for potentials reversals of -1.18 and -1.19 V (in all baths).

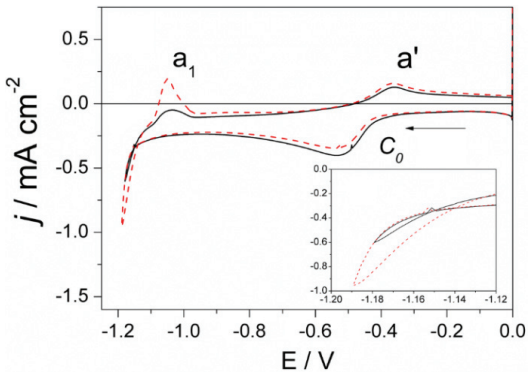

Figure 2. Reversed-sweep voltammograms for Pt in solution of 0.10 M $ZnSO_4$ + 0.14 M $MnSO_4$ + BA 0.08 M + 0.08 M GLY: reversal at -1.18 and -1.19 V (inset: expanded region).

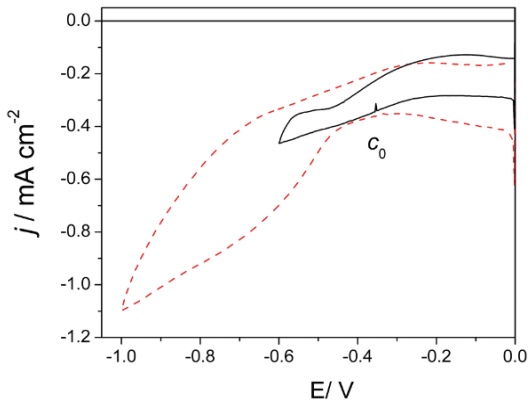

Figure 3. Reversed-sweep voltammograms for Pt in solution of 0.10 M $ZnSO_4$ + 0.14 M $MnSO_4$ + BA 0.08 M + 0.08 M GLY: reversal at -0.6 and -1.0 V (stirred at 5 Hz).

Fletcher et al. (1983) reported that crossover suggests a nucleation process. Here, the Mn deposition occurs at ~-1.53 V, which implies that the initial deposition of zinc occurred soon after -1.18 V in the negative sweep, i.e., nucleation and primary growth of zinc occurs at c_o. Thus, the wave c_o (Figure 2) likely corresponds to the HER and initial zinc bulk deposition. GLY is adsorbed on the electrode surface, and the crossover potential (E_{c1}) shifted by ~30 mV in the negative direction. The E_{pa} shifted ~30 mV in the positive direction with increasing of GLY concentrations. Figure 3 only shows the crossover pertaining to bath A, and the results were similar for all other baths.

Figure 4 shows that when the sweep was reversed at a limit potential more negative than -1.19 V, an anodic peak (a_1) is seen due to the dissolution of electrodeposits. Importantly, the a_1 indicates primary nucleation and growth of Zn (region c_o), and this is followed by secondary nucleation and subsequent growth of Zn (peak c_1). The latter occurs on the top of the initial bulk Zn deposit. These results corroborate with Túlio and Carlos (2009), Oliveira and Carlos (2008) and Carvalho, Rubin, and Carlos (2010). Importantly, crossovers were noted at potentials more negative than ~-1.20 V suggesting that both zinc and manganese nucleation and growth processes occurred. In addition, the a_1 charge density increased because the amount of metal deposited increased as the negative sweep was reversed at potentials more negative than -1.33 V.

Figure 5 shows the current efficiency (CE) during chronoamperometric deposition of Zn-Mn alloy at -1.53 V and q_d = 10.20 mA cm^{-2} from baths A-H. The CE of electrodeposition process Zn-Mn increases when the GLY concentration ranged from 4.78 to 33.08%. The final increase at [GLY] = 0.63 M was enhanced by raising the concentration of BA threefold giving a CE value of 40.64%. The addition of GLY inhibited the HER, and this inhibition was strongest in the bath containing a three-fold higher concentration of BA and high GLY concentration. These results demonstrated that BA and GLY compete with H^+ ions for active sites on the surface of the electrode.

Characterization of Zn-Mn electrodeposits by scanning electron microscopy and X-ray diffraction

Figure 6 shows the SEM micrographs of electrodeposits produced chronoamperometrically at -1.53 V from baths A-H. The potential is in the region between the two deposition peaks (c_1 and c_2), and it was chosen to coincide with the one used by Rubin et al. (2012). The deposits obtained in the presence of 0.08 M BA were not uniform (with GLY ranging from 0.08 to 0.48 M); they were formed by dendritic crystallites of different shapes and sizes. However, the crystallites were not uniform but were rather quite globular with some clusters of crystallites at 0.08 M BA and 0.63 M GLY (see Figure 6f). Increasing the BA concentration was not beneficial (see Figure 6g-h) because the size of crystallites was higher than those formed in 0.08 M BA and GLY (see Figure 6e-f). The crystallites were small but had more refined grains in the presence of 0.63 M GLY at both BA concentrations (baths F and H). These results imply that GLY acted as a deposit brightener. The zinc-manganese nucleation and growth processes were progressive because crystallites of various sizes were observed. Even so, the deposits obtained at this potential were dark gray.

The film deposited in the presence of 0.24 M GLY (see Figure 6c) was compared to that produced by Rubin et al. (2012) in 0.24 M BSC (at -1.60 V and q_d = 10.20 C cm^{-2}). Rubin et al. (2012) showed more compact and coalesced rounded plates, and the deposits did not contain Mn. In contrast, Diaz-Arísta et al. (2009) demonstrated that the deposits formed were compact with a small grain size, while Sylla et al. (2005) found that the film morphologies were cauliflower-like.

The X-ray diffraction patterns of the Zn-Mn films show typical diffraction patterns for the Zn-Mn deposits produced at -1.53 V from solutions in Table 1 (see Figure 7 and S4-10 in the Supplementary Material). These results indicate that the films were mainly composed of pure Zn and Mn as well as alloys at several compositions: $MnZn_{13}$, $Mn_{0.52}Zn_{0.48}$, $Mn_{0.27}Zn_{0.73}$, and $Mn_{1.08}Zn_{2.92}$ plus some oxides such as ZnO, MnO, $ZnMn_2O_4$, Mn_2O_4, Mn_3O_4, $MnZnO_3$ and manganese hydride ($MnH_{0.8}$). Nevertheless, those electrodeposited from baths C, D and E also showed compounds that were not found in the other electrodeposits: Pt (bath C); Mn_2O_3 and Pt (bath D) and Mn_2O_3 (bath E). All diffraction patterns of the electrodeposits were compared to the expected values from the JCPDS database (Joint Committee on Powder Diffraction Standards [JCPDS], 2000) for peaks with relative intensities greater than 10%.

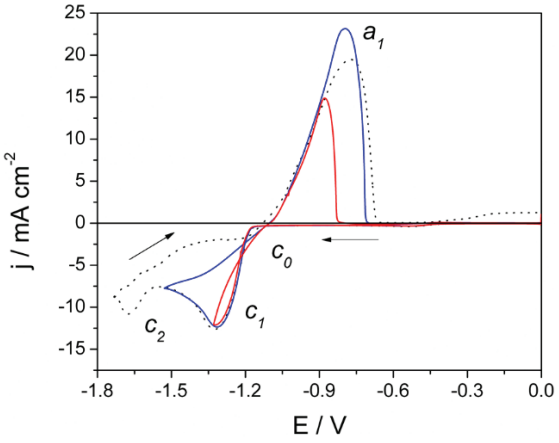

Figure 4. Reversed-sweep voltammograms for Pt in solution of 0.10 M $ZnSO_4$ + 0.14 M $MnSO_4$ + BA 0.08 M + 0.08 M GLY: reversal at -1.33, -1.53 and -1.74 V (stirred at 5 Hz).

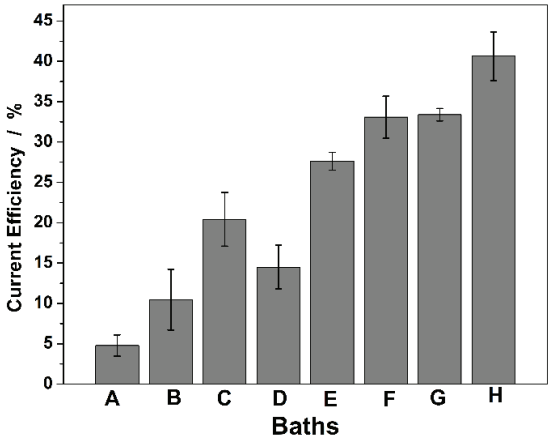

Figure 5. Current efficiency of the Zn-Mn alloy deposition process obtained chronoamperometrically in eight different deposition baths (at -1.53 V and q_d = 10.20 mA cm^{-2}).

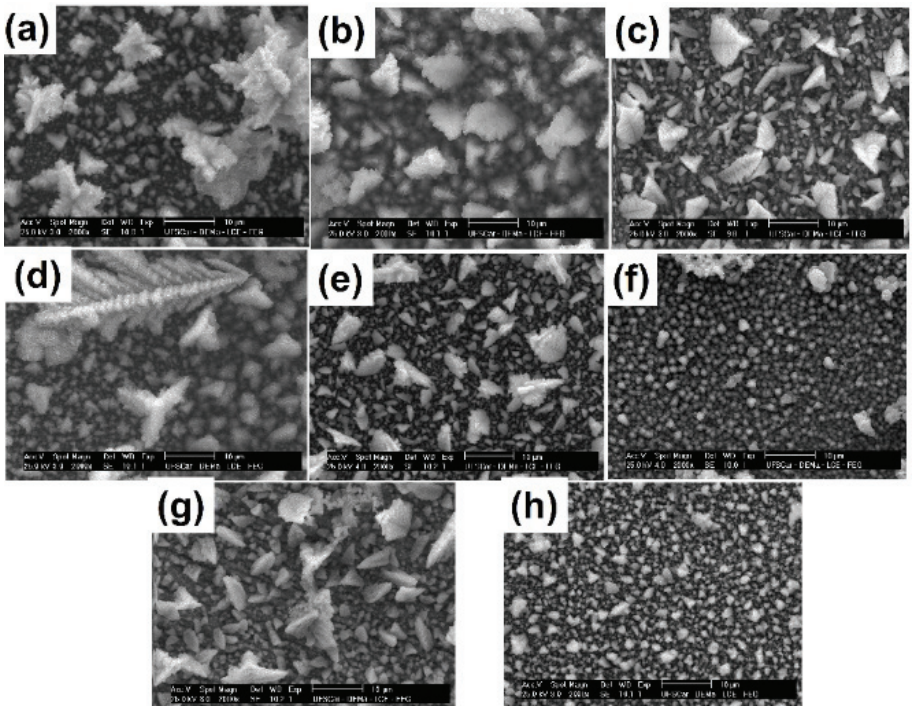

Figure 6. SEM of electrodeposits obtained chronoamperometrically from E = -1.53 V, q_{dep} = 10.20 C cm^{-2} from baths of $ZnSO_4$ (0.10 M) + $MnSO_4$ (0.14 M) with various contents of additives: (a) bath A; (b) bath B; (c) bath C; (d) bath D; (e) bath E; (f) bath F; (g) bath G; and (h) bath H. Magnification 2.000 x.

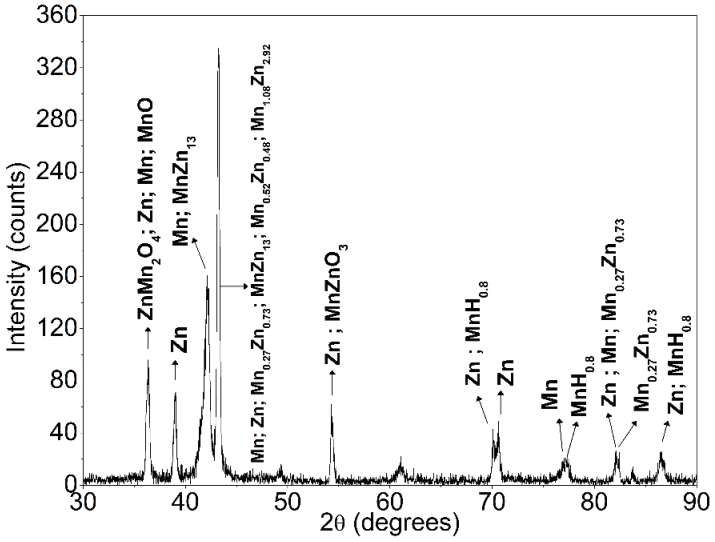

Figure 7. X-ray diffraction patterns of the films of Zn-Mn deposited chronoamperometrically in bath H at -1.53 V, with q_d = 10.20 cm^{-2} (2ϴ scanned at 2° $min.^{-1}$).

Conclusion

This research showed that GLY and BA were adsorbed on the electrode surface and inhibited the co-deposition of Mn and Zn, while GLY inhibited the formation of manganese oxides. The deposits were not uniform with dendrites of different shapes and sizes indicating globular crystallites with some small aggregates. In this deposit, GLY acted as a brightener, and the deposit was less rough. Moreover, XRD structural analysis showed that films consist of pure metals, oxides and Zn-Mn alloys of various compositions-the composition of the phases did not change in the presence of GLY.

Acknowledgements

This research has been supported by Fapesp (Proc. No. 2009/01665-0). Special thanks to Drª Ivani A. Carlos (from UFSCar Chemistry Department, Brazil) for her very valuable critical comments. R. B. Viana also thanks Capes for the research fellowship.

References

Ananth, M. V., & Parthasaradhy, N. V. (1996). Magnetization behaviour of electrodeposited Zn-Mn alloy. *Materials Science and Engineering: B, 40*(1), 19-23. doi: 10.1016/0921-5107(96)01537-1

Boshkov, N., Petrov, K., & Vitkova, S. (2002). Corrosion products of zinc-manganese coatings: part III-Double protective action of manganese. *Metal Finishing, 100*(6), 98-100. doi: 10.1016/S0026-0576(02)80445-7

Boshkov, N., Petrov, K., Vitkova, S., & Raichevsky, G. (2005). Galvanic alloys Zn–Mn -composition of the corrosion products and their protective ability in sulfate containing medium. *Surface and Coatings Technology, 194*(2-3), 276-282. doi: 10.1016/j.surfcoat.2004.09.016

Bozzini, B., Accardi, V., Cavallotti, P. L., & Pavan, F. (1999). Electrodeposition and plastic behavior of low-manganese zinc-manganese alloy coatings for automotive applications. *Metal Finishing, 97*(5), 33. doi: 10.1016/S0026-0576(00)80031-8

Bozzini, B., Griskonis, E., Fanigliulo, A., & Sulcius, A. (2002). Electrodeposition of Zn-Mn alloys in the presence of thiocarbamide. *Surface and Coatings Technology, 154*(2-3), 294-303. doi: 10.1016/S0257-8972(02)00010-5

Brenner, A. (1963). *Electrodeposition of alloys* (vol. 2). New York, NY: Academic Press.

Bucko, M., Culliton, D., Betts, A. J., & Bajat, J. B. (2017) The electrochemical deposition of Zn–Mn coating from choline chloride–urea deep eutectic solvent. *Transactions of the IMF, 95*(1), 60-64. doi: 10.1080/00202967.2017.1255412

Bucko M., Stevanović, S., & Bajat, J. (2018) Tailoring the corrosion resistance of Zn-Mn coating by electrodeposition from deep eutectic solvents. *Zastita materijala, 59*(2), 173-181. doi: 10.5937/zasmat1802173b

Bucko, M., Lacnjevac, U., & Bajat, J. (2013a). The influence of substituted aromatic aldehydes on the electrodeposition of Zn-Mn alloy. *Journal of the Serbian Chemical Society, 78*(10), 1569-1581. doi: 10.2298/jsc130118025b

Bucko, M., Mišković-Stanković, V., Rogan, J., & Bajat, J. B. (2015). The protective properties of epoxy coating electrodeposited on Zn-Mn alloy substrate. *Progress in Organic Coatings, 79*, 8-16. doi: 10.1016/j.porgcoat.2014.10.010

Bucko, M., Rogan, J., Stevanović, S. I., Peric-Grujic, A., & Bajat, J. B. (2011). Initial corrosion protection of Zn–Mn alloys electrodeposited from alkaline solution. *Corrosion Science, 53*(9), 2861-2871. doi: 10.1016/j.corsci.2011.05.039

Bucko, M., Rogan, J., Stevanovic, S. I., Stankovic, S., & Bajat, J. B. (2013b). The influence of anion type in electrolyte on the properties of electrodeposited ZnMn alloy coatings. *Surface and Coatings Technology, 228*, 221-228. doi: 10.1016/j.surfcoat.2013.04.032

Carvalho, M. F., Rubin, W., & Carlos, I. A. (2010). Study of the influence of the polyalcohol mannitol on zinc electrodeposition from an alkaline bath. *Journal of Applied Electrochemistry, 40*(9), 1625-1632. doi: 10.1007/s10800-010-0148-0

Chen, P. Y., & Hussey, C. L. (2007). The electrodeposition of Mn and Zn-Mn alloys from the room-temperature tri-1-butylmethylammonium bis[(trifluotomethane)sulfonyl]imide ionic liquid. *Electrochimica Acta, 52*(5), 1857-1864. doi: 10.1016/j.electacta.2006.07.049

Chung, P. P., Cantwell, P. A., Wilcox, G. D. & Critchlow, G. W. (2008) Electrodeposition of zinc–manganese alloy coatings from ionic liquid electrolytes. *Transactions of the IMF, 86*(4), 211-219. doi: 10.1179/174591908X327572

Claudel, F., Stein, N., Allain, N., Tidu, A., Hajczak, N., Lallement, R., & Close, D. (2019) Pulse electrodeposition and characterization of Zn–Mn coatings deposited from additive-free chloride electrolytes. *Journal of Applied Electrochemistry, 49*(5-8), 399-411. doi: 10.1007/s10800-019-01295-1

Close, D., Stein, N., Allain, N., Tidu, A., Drynski, E., Merkleinc, M., & Lallement, R. (2016). Electrodeposition, microstructural characterization and anticorrosive properties of Zn-Mn alloy coatings from acidic chloride electrolyte containing 4-hydroxybenzaldehyde and ammonium thiocyanate. *Surface and Coatings Technology, 298*, 73-82. doi: 10.1016/j.surfcoat.2016.04.043

Díaz-Arista, P., Ortiz, Z. I., Ruiz, H., Ortega, R., Meas, Y., & Trejo, G. (2009). Electrodeposition and characterization of Zn-Mn alloy coatings obtained from a chloride-based acidic bath containing ammonium thiocyanate as an additive. *Surface and Coatings Technology, 203*(9), 1167-1175. doi: 10.1016/j.surfcoat.2008.10.015

Fashu, S., Gu, C. D., Zhang, J. L., Zheng, H., Wang, X. L., & Tu, J. P. (2015). Electrodeposition, morphology, composition, and corrosion performance of Zn-Mn coatings from a deep eutectic solvent. *Journal of Materials Engineering and Performance, 24*(1), 434-444. doi: 10.1007/s11665-014-1248-5

Fletcher, S., Halliday, C. S., Gates, D., Westcott, M., Lwin, T., & Nelson, G. (1983). The response of some nucleation/growth processess to triangular scans of potential. *Journal of Electroanalytical Chemistry and Interfacial Electrochemistry, 159*(2), 267-285. doi: 10.1016/S0022-0728(83)80627-5

Ganesan, S., Prabhu, G., & Popov, B. N. (2014). Electrodeposition and characterization of Zn□Mn coatings for corrosion protection. *Surface and Coatings Technology, 248*, 143-151. doi: 10.1016/j.surfcoat.2013.10.062

Griskonis, E., & Sulcius, A. (2005). Influence of selenates on the electrodeposition of zinc-manganese alloy. *Bulletin of Electrochemistry, 21*(12), 561-565.

Joint Committee on Powder Diffraction Standards [JCPDS]. (2000). *International Centre for Diffraction Data. Powder diffraction file-PDF-2*. Harrisburg, PA: JCPDS.

Louki, N., & Feki, M. (2017a). Zn–Mn alloy coatings from acidic chloride bath: Effect of deposition conditions on the Zn–Mn electrodeposition-morphological and structural characterization. *Applied Surface Science, 410*, 574-584. doi: 10.1016/j.apsusc.2017.02.075

Loukil, N, & Feki, M (2017b) Synergistic effect of triton X 100 and 3-hydroxybenzaldehyde on Zn-Mn electrodeposition from acidic chloride bath. *Journal of Alloys and Compounds, 719*, 420–428. doi: 10.1016/j.jallcom.2017.05.142

Marin-Sanchez, M., Ocon, P., Conde, A., & Garcia, I. (2014). Electrodeposition of Zn-Mn coatings on steel from 1-ethyl-3-methylimidazolium bis (trifluoromethanesulfonyl) imide ionic liquid. *Surface and Coatings Technology, 258*, 871-877. doi: 10.1016/j.surfcoat.2014.07.064

Muller, C., Sarret, M., & Andreu, T. (2003a). Electrodeposition of ZnMn alloys using pulse plating. *Journal of the Electrochemical Society, 150*(11), C772-C776. doi: 10.1149/1.1614270

Muller, C., Sarret, M., & Andreu, T. (2003b). ZnMn alloys obtained using pulse, reverse and superimposed current modulations. *Electrochimica Acta, 48*(17), 2397-2404. doi: 10.1016/S0013-4686(03)00253-6

Oliveira, E. M., & Carlos, I. A. (2008). Voltammetric and morphological characterization of zinc electrodeposition from acid electrolytes containing boric-polyalcohol complexes. *Journal of Applied Electrochemistry, 38*(9), 1203-1210. doi: 10.1007/s10800-008-9534-2

Ortiz, Z. I., Diaz-Arista, P., Meas, Y., Ortega-Borges, R., & Trejo, G. (2009). Characterization of the corrosion products of electrodeposited Zn, Zn-Co and Zn-Mn alloys coatings. *Corrosion Science, 51*(11), 2703-2715. doi: 10.1016/j.corsci.2009.07.002

Pourbaix, M. (1966). *Atlas of electrochemical equilibria in aqueous solutions* (2nd ed.). Oxford, GB: Pergamon Press Ltda.

Rubin, W., Oliveira, E. M., & Carlos, I. A. (2012). Study of the influence of a boric–sorbitol complex on Zn–Mn electrodeposition and on the morphology, chemical composition, and structure of the deposits. *Journal of Applied Electrochemistry, 42*(1), 11-20. doi: 10.1007/s10800-011-0365-1

Silva, P. S., Schmitz, E. P. S., Spinelli, A., & Garcia, J. R. (2012). Electrodeposition of Zn and Zn-Mn alloy coatings from an electrolytic bath prepared by recovery of exhausted zinc-carbon batteries. *Journal of Power Sources, 210*, 116-121. doi: 10.1016/j.jpowsour.2012.03.021

Sulcius, A., Griskonis, E., & Diaz-Arista, P. (2009). Influence of ammonium selenate and thiourea mixture on mechanical properties and morphology of Zn-Mn alloy coatings electrodeposited from sulphate-citrate bath. *Transactions of the IMF, 87*(5), 254-258. doi: 10.1179/002029609x12483598222682

Sylla, D., Rebere, C., Gadouleau, M., Savall, C., Creus, J., & Refait, P. H. (2005). Electrodeposition of Zn–Mn alloys in acidic and alkaline baths. Influence of additives on the morphological and structural properties. *Journal of Applied Electrochemistry, 35*(11), 1133-1139. doi: 10.1007/s10800-005-9001-2

Touazi, S., Bučko, M., Makhloufi, L., Lega,t A., & Bajat, J. B. (2016) The electrochemical behavior of Zn–Mn alloy coating in carbonated concrete solution. *Surface Review and Letters, 23*(4), 1650030. doi: 10.1142/s0218625x1650030x

Túlio, P. C., & Carlos, I. A. (2009). Effects of SiC and Al_2O_3 particles on the electrodeposition of Zn, Co and ZnCo. I. Electrodeposition in the absence of SiC and Al_2O_3. *Journal of Applied Electrochemistry, 39*(2), 283-291. doi: 10.1007/s10800-008-9670-8

Wilcox, G. D., & Gabe, D. R. (1993). Electrodeposited zinc alloy coatings. *Corrosion Science, 35*(5-8), 1251-1258. doi: 10.1016/0010-938x(93)90345-h

Wykpis, K., Bierska-Piech, B., & Kubisztal, J. (2014). Electrodeposition of Zn-Mn coatings from a sulphate bath in the presence of complexing additives. *Surface and Interface Analysis, 46*(10-11), 740-745. doi: 10.1002/sia.5477